Published March 7, 2011

miR-24 inhibits apoptosis and represses Bim in mouse cardiomyocytes

Li Qian,[1,2,3] Linda W. Van Laake,[1,2,3,5] Yu Huang,[1,2,3] Siyuan Liu,[4] Michael F. Wendland,[4] and Deepak Srivastava[1,2,3]

[1]Gladstone Institute of Cardiovascular Disease, [2]Department of Pediatrics, [3]Department of Biochemistry and Biophysics, and [4]Department of Radiology and Biomedical Imaging, University of California, San Francisco, San Francisco, CA 94143
[5]University Medical Center Utrecht, Utrecht University, 3508 GA Utrecht, Netherlands

Acute myocardial infarction (MI) involves necrotic and apoptotic loss of cardiomyocytes. One strategy to salvage ischemic cardiomyocytes is to modulate gene expression to promote cell survival without disturbing normal cardiac function. MicroRNAs (miRNAs) have emerged as powerful regulators of multiple cellular processes, including apoptosis, suggesting that regulation of miRNA function could serve a cardioprotective function. In this study, we report that miR-24 (miRNA-24) expression is down-regulated in the ischemic border zone of the murine left ventricle after MI. miR-24 suppresses cardiomyocyte apoptosis, in part by direct repression of the BH3-only domain–containing protein Bim, which positively regulates apoptosis. In vivo expression of miR-24 in a mouse MI model inhibited cardiomyocyte apoptosis, attenuated infarct size, and reduced cardiac dysfunction. This antiapoptotic effect on cardiomyocytes in vivo was partially mediated by Bim. Our results suggest that manipulating miRNA levels during stress-induced apoptosis may be a novel therapeutic strategy for cardiac disease.

CORRESPONDENCE
Deepak Srivastava:
dsrivastava@gladstone.ucsf.edu

Abbreviations used: AAR, area at risk; ANF, atrial natriuretic factor; BNP, brain natriuretic peptide; BZ, border zone; DZ, distant zone; ECG, electrocardiography; EF, ejection fraction; IZ, infarct zone; LV, left ventricle; MI, myocardial infarction; miRNA, microRNA; MRI, magnetic resonance imaging; mRNA, messenger RNA; PFA, paraformaldehyde; PI, propidium iodide; qPCR, quantitative PCR; siRNA, small interfering RNA; SV, stroke volume; TTC, triphenyltetrazolium chloride; TUNEL, Tdt-mediated dUTP-biotin nick end labeling; UTR, untranslated region.

Myocardial infarction (MI), caused by acute occlusion of the coronary artery, is one of the leading causes of death and disability worldwide (Mackman, 2008). Over seven million people die each year from acute MI or progressive cardiac dysfunction after coronary artery occlusion. MI induces cardiac cell death and ischemic stress in surviving myocytes bordering the region of infarct (border zone [BZ]), which triggers left ventricle (LV) remodeling, leading to dilation, hypertrophy, and fibrosis (Swynghedauw, 1999). Scar formation and pathological LV remodeling result in cardiac dysfunction and eventually lead to heart failure (Swynghedauw, 1999). Apoptosis (programmed cell death) contributes significantly to cardiomyocyte loss during acute MI, particularly in the BZ, and during subsequent remodeling events (Kang et al., 2000; Kitsis et al., 2007). Because cardiomyocytes are terminally differentiated and have little potential for division, controlling the loss of cardiomyocytes after injury holds potential therapeutic value.

Posttranscriptional regulation involving a class of small noncoding RNAs known as microRNAs (miRNAs; Ambros, 2003; Zhao and Srivastava, 2007; Ruvkun, 2008; Bartel, 2009) has emerged as a major regulator of numerous cellular processes, including those involved in the heart. Through imperfect sequence-specific binding to their messenger RNA (mRNA) targets, miRNAs negatively influence the expression of proteins by destabilizing target mRNAs or inhibiting translation (Ambros, 2003; Zhao et al., 2005; Zhao and Srivastava, 2007; Ruvkun, 2008; Bartel, 2009). miRNAs control various aspects of heart development and function, including cell proliferation (Zhao et al., 2005, 2007; Chen et al., 2006), lineage differentiation (Kwon et al., 2005; Sokol and Ambros, 2005; Chen et al., 2006; Ivey et al., 2008), and cardiac conduction (Yang et al., 2007; Zhao et al., 2007). Several miRNAs are dysregulated during cardiac remodeling after injury or stress (van Rooij et al., 2006, 2007, 2008; Carè et al., 2007), including

L. Qian and L.W. Van Laake contributed equally to this paper.

The Rockefeller University Press $30.00
J. Exp. Med. Vol. 208 No. 3 549-560
www.jem.org/cgi/doi/10.1084/jem.20101547

Supplemental Material can be found at:
http://jem.rupress.org/content/suppl/2011/03/04/jem.20101547.DC1.html

Published March 7, 2011

miR-29 (miRNA-29) and miR-21 (Thum et al., 2008; van Rooij et al., 2008; Dong et al., 2009).

In this study, we identify miR-24 as an antiapoptotic miRNA that is down-regulated in the ischemic zones of the LV after acute MI. We show that miR-24 directly targets the proapoptotic protein Bim within cardiomyocytes for repression and inhibits apoptosis in vitro and in vivo. In vivo delivery of miR-24 after MI reduced scar size and improved long-term cardiac function.

RESULTS

miR-24 suppresses apoptosis

In an effort to identify miRNAs dysregulated within hours after MI, we found that miR-24 was highly down-regulated in the ischemic BZ but not in the nonischemic distant zone (DZ) of the LV 24 h after MI (Fig. 1, A–C). miR-23a and miR-23b, encoded by the same cluster as miR-24, were also down-regulated at the BZ but to a lesser extent; in contrast, expression of miR-27a and miR-27b, which are also clustered with miR-24, was not altered at the BZ (Fig. S1 A). miR-24 expression was normally enriched in the adult mouse heart, specifically in sorted cardiac myocyte and fibroblast populations but not in endothelial cells (Fig. S1, B–H). Interestingly, miR-24 down-regulation was attenuated over time, and its expression was restored back to wild-type levels by 4 wk after MI (Fig. 1, A and B). We quantified apoptotic cardiomyocytes in the BZ and DZ regions over time (Fig. 1, D and E) and found a close correlation between down-regulation of miR-24 and increase in apoptosis (Fig. 1, A–E).

To investigate miR-24 function, we transfected primary cardiomyocytes with chemically synthesized double-stranded oligonucleotides that mimic the function of endogenous mature miR-24 (miR-24 mimic) or modified antisense oligoribonucleotides that inhibit miR-24 function (miR-24 inhibitor). Transfection efficiency (~80%) was monitored by FACS analysis of cotransfected Alexa Fluor 488–conjugated oligonucleotides (Fig. S2, A and B), expression levels were evaluated by real-time quantitative PCR (qPCR; Fig. S2, C and D), and functional activity of transfected miR-24 oligonucleotides was measured by luciferase sensor experiments (Fig. S2 E). Additional miR-24 mimic and inhibitor controls in which the seed sequence of miR-24 was mutated were used (see Materials and methods).

miR-24 expression in cardiomyocytes increased cell number by 53%, and inhibition of miR-24 function decreased cell number by 45% 48 h after transfection. We did not observe a difference in cell number upon introduction of control mimic, control inhibitor, or mock transfection (Lipofectamine only). However, the number of live cells (propidium iodide$^-$ [PI$^-$]) positive for AnnexinV, an early apoptosis marker, was increased when miR-24 was inhibited. Conversely, fewer AnnexinV$^+$PI$^-$ cells were seen when miR-24 was overexpressed (Fig. S3, A–D). During later apoptosis, DNA fragmentation results from activation of endonucleases (Hengartner, 2000). Using TUNEL (Tdt-mediated dUTP-biotin nick end labeling) staining to detect fragmented DNA in cardiomyocytes after overexpression or inhibition of miR-24, we found that miR-24 negatively regulated this marker of apoptosis (Fig. 1, F–I). Quantification for activated Caspase 3–positive cardiomyocytes further confirmed the results (Fig. 1, J and K). Cell cycle patterns were similar among miR-24 mimic– and miR-24 inhibitor–expressing and control cells (Fig. S3, E and F).

miR-24 directly targets Bim for repression in cardiomyocytes

Because miR-24 inhibited cardiomyocyte apoptosis, we searched for direct downstream effectors/targets by which miR-24 exerts its function. We used established computational algorithms to predict potential miR-24 target genes (Krek et al., 2005; Rajewsky, 2006; Bartel, 2009) and performed gene expression analyses. Among down-regulated genes, the proapoptotic Bcl2 family protein Bim was a strong candidate target based on the presence of predicted miR-24 binding sites. Bim mediates mitochondrial and ER stress–induced apoptosis, and its levels are controlled by multiple mechanisms, including transcriptional and posttranscriptional events such as phosphorylation, ubiquitination, proteasomal degradation, and miRNA regulation (i.e., miR-17-92; Dijkers et al., 2000; Puthalakath and Strasser, 2002; Ley et al., 2005; Puthalakath et al., 2007; Ventura et al., 2008; Xiao et al., 2008).

To test whether Bim is also regulated by miR-24, qPCR and Western blots of cardiomyocytes transfected with miR-24 mimic or inhibitor were performed. mRNA and protein levels of Bim were down-regulated when miR-24 was overexpressed, whereas inhibiting miR-24 function resulted in up-regulation of Bim (Fig. 2, A and B). We identified two conserved miR-24 binding sites in the Bim mRNA 3′ untranslated region (UTR; Fig. 2 C). To test whether miR-24 repressed Bim by binding to these sites, the *Bim* 3′ UTR was inserted into the 3′ UTR of a luciferase reporter, downstream of the coding region. The constitutively active reporter was cotransfected with miR-24 mimic, inhibitor, or miR-24 cloned in an expression vector (pEF–miR-24) into HeLa cells. Transfection of the *Bim* 3′ UTR chimeric luciferase reporters with miR-24 (miR-24 mimic or pEF–miR-24) resulted in a decrease in luciferase activity, whereas cotransfection with miR-24 inhibitor resulted in increased luciferase activity (Fig. 2 C). Mutations of the miR-24 binding sites in the Bim 3′ UTR abolished miR-24 responsiveness (Fig. 2 C), suggesting that miR-24 represses *Bim* by physically binding to its 3′ UTR. The same luciferase experiment was performed in cardiomyocytes, confirming the results from HeLa cells (Fig. S3 G).

We investigated whether miR-24 repression of Bim in primary cardiomyocytes could account for some of the effects of miR-24 on the apoptotic pathway. Bim knockdown led to a reduction in the number of apoptotic cells (Fig. 2 D and not depicted), phenocopying overexpression of miR-24. Most importantly, the increase in apoptotic cell number caused by inhibition of miR-24 could be reversed by knockdown of *Bim* (Fig. 2 E and not depicted), suggesting an epistatic relationship between miR-24 and *Bim*.

Published March 7, 2011

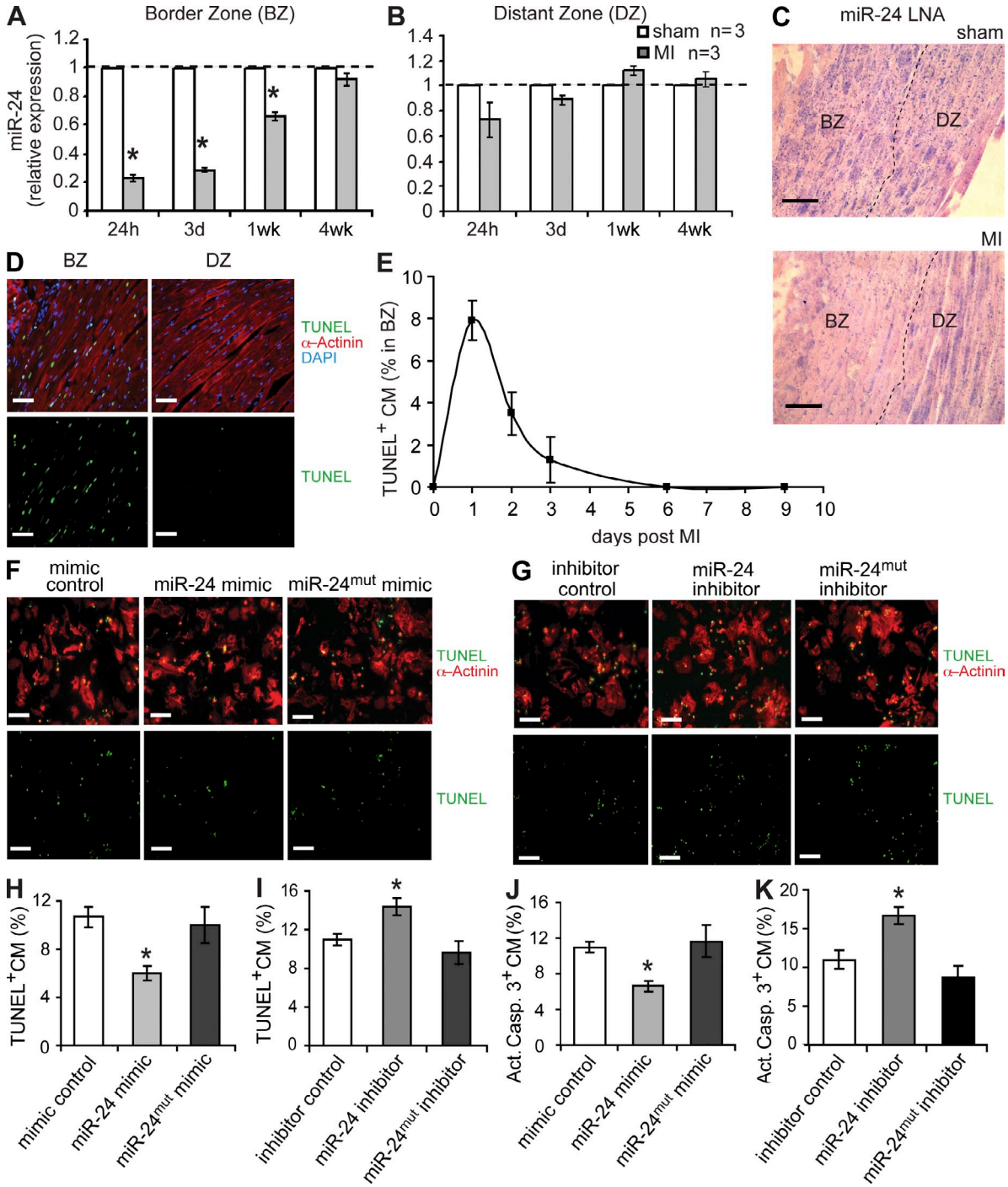

Figure 1. miR-24 is down-regulated early after MI and inhibits apoptosis. (A and B) qPCR of miR-24 was performed on RNA extracted from the BZ and DZ of hearts 24 h, 3 d, and 1 and 4 wk after coronary artery ligation (MI) or sham surgery. (C) In situ hybridization using miR-24 locked nucleic acid (LNA) probe on heart sections from MI and sham operated mice 24 h after surgery. (D) TUNEL staining of infarcted hearts 24 h after coronary artery ligation. Cardiomyocytes were costained with antibody to α-Actinin. DAPI was used for nuclear staining. (E) Percentage of TUNEL-positive cardiomyocytes (CM) at BZ of hearts over time after MI. $n = 3$ for each time point. (F and G) TUNEL and α-Actinin staining on primary cardiomyocytes transfected with mimic control, miR-24 mimic, or miR-24^{mut} mimic (F) or transfected with inhibitor control, miR-24 inhibitor, or miR-24^{mut} inhibitor (G). (H and I) Quantification of percentage of TUNEL-positive cardiomyocytes in F and G. (J and K) Quantification of percentage of Caspase 3–positive cardiomyocytes. All experiments were repeated three times (technical triplicates) with biological triplicates ($n = 3$). Error bars indicate SEM (*, $P < 0.05$). Bars, 50 µm.

Published March 7, 2011

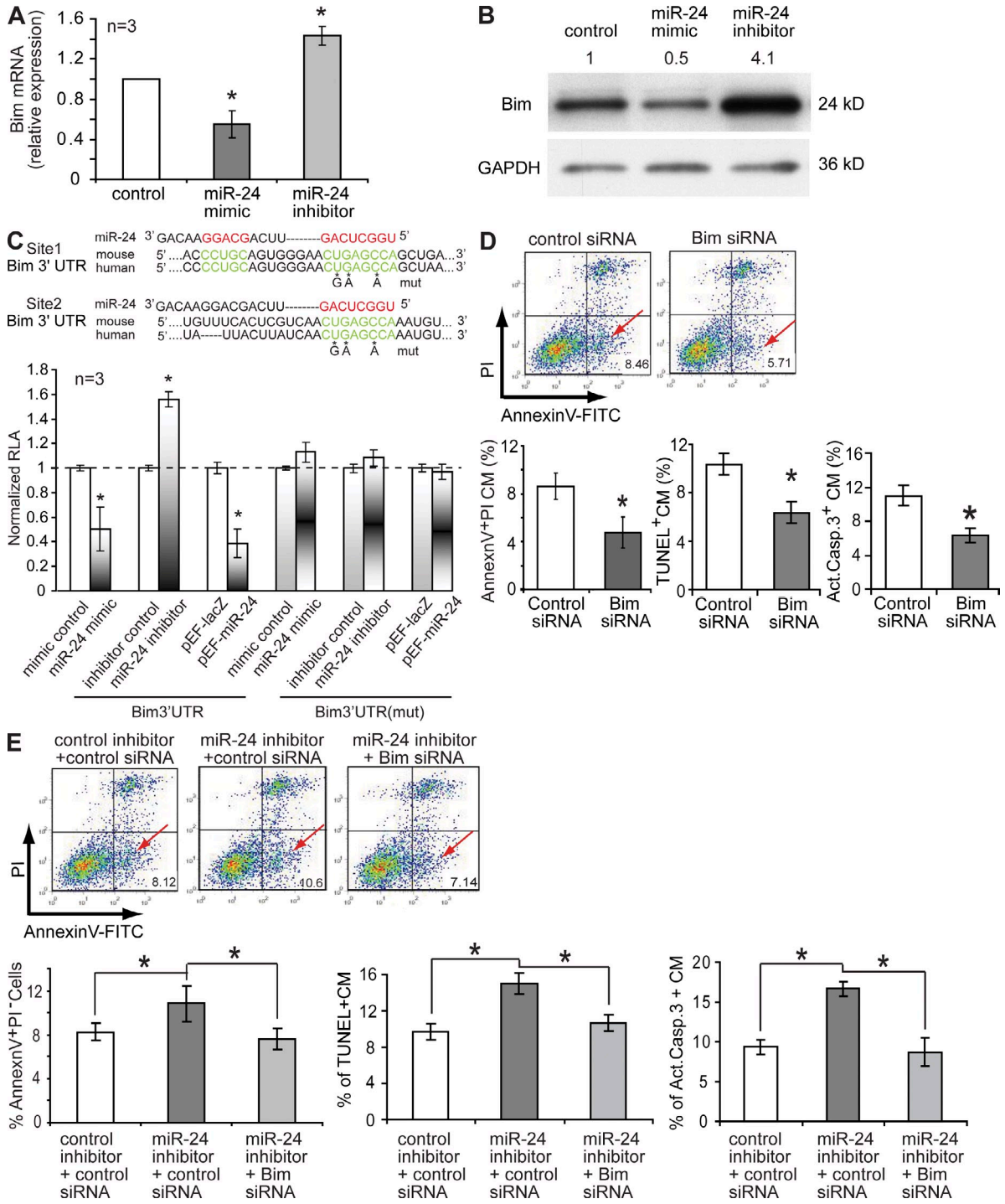

Figure 2. Bim is a direct target of miR-24. (A) qPCR of *Bim* mRNA from cardiomyocytes transfected with control (mock transfection with Lipofectamine 2000 only), miR-24 mimic, or miR-24 inhibitor. (B) Western blot comparing protein levels of Bim in control (mock transfection) and miR-24 mimic– or miR-24 inhibitor–expressing cells. Quantification compared with control (set as 1) is shown above the panel. (C) Conserved miR-24 binding sites in the Bim 3′ UTR and relative luciferase activity (RLA) in HeLa cells expressing miR-24 mimic, miR-24 precursor (in expression vector, pEF–miR-24), or inhibitor compared with control. Base pairs highlighted in color (miR-24 in red and Bim 3′ UTR in green) are seed sequences that are complimentary between miRNA and target. Mutations in miR-24 binding sites for luciferase assay in 3′ UTR are indicated. Controls are set up as 1, indicated by the dashed line. (D) Primary cardiomyocytes (CM) expressing control siRNA or Bim siRNA were stained with AnnexinV, PI, TUNEL, or activated Caspase 3. Dot plots show representative staining by flow cytometry, and arrows indicate the quadrant of AnnexinV$^+$PI$^-$ apoptotic cells. (E) Primary cardiomyocytes co-transfected with *Bim* siRNA and miR-24 inhibitor or control inhibitor were stained with AnnexinV, PI, TUNEL, or activated Caspase 3. Dot plots show representative staining by flow cytometry, and arrows indicate the quadrant of AnnexinV$^+$PI$^-$ apoptotic cells. All experiments were repeated three times (technical triplicates) with biological triplicates ($n = 3$). Bar graphs show mean ± SEM (*, $P < 0.05$).

Published March 7, 2011

In vivo delivery of miR-24 inhibits apoptosis in a mouse MI model

Apoptotic signals are propagated in response to ischemic stress in the heart. Thus, we speculated that the extensive apoptosis after MI may be enhanced by the decreased levels of miR-24. We used a Lipofectamine-mediated in vivo transfection method (Yang et al., 2007) to locally deliver miR-24 mimics to the infarcted hearts of mice in an effort to restore miR-24 levels. To validate the delivery efficiency, fluorescently labeled oligonucleotides mixed with Lipofectamine were injected. By 24 h after the procedure, strong fluorescence around the injection area revealed efficient uptake (Fig. S4, A–C). qPCR and in situ hybridization of miR-24 revealed high expression levels in the injected areas (Fig. S4, D and E), although it is difficult to directly assess the functionality of injected oligonucleotides in vivo.

To determine whether miR-24 mimic treatment could inhibit ischemia-induced apoptosis of cardiomyocytes in vivo, we combined TUNEL labeling with the cardiomyocyte marker α-Actinin on infarcted mouse hearts treated with miR-24 or control mimics. The percentage of TUNEL-positive (apoptotic) cardiomyocytes in the BZs along the infarct area was 62% ($P < 0.05$) lower in animals treated with miR-24 mimic than in control mimic–treated mice (Fig. 3, A and B). This result was confirmed by using another apoptotic marker, activated Caspase 3, in combination with α-Actinin (Fig. 3 C and not depicted). In parallel, we assayed for phosphorylated histone H3 (pH3) and α-Actinin to compare the difference in the progression of cardiomyocyte mitosis among the two groups of mice. We detected no mitotic cardiomyocytes in either miR-24 mimic– or control mimic–treated mice (unpublished data). To determine whether the inhibition of apoptosis by miR-24 affected the degree of myocardial damage, we performed Evans blue/triphenyltetrazolium chloride (TTC) double staining to assess the area at risk (AAR) and the infarct size of myocardium 24 h after coronary ligation. Treatment of miR-24 led to a decrease in infarct size but no change in AAR (Fig. 3, D and E), suggesting that miR-24 expression reduced cardiac damage shortly after MI.

In vivo delivery of miR-24 reduces cardiac dysfunction in a mouse MI model

Acute MI in mice causes myriad hemodynamic stresses, which trigger left ventricular remodeling and eventually lead to functional decompensation and heart failure (Lutgens et al., 1999; Bock-Marquette et al., 2004). We hypothesized that a

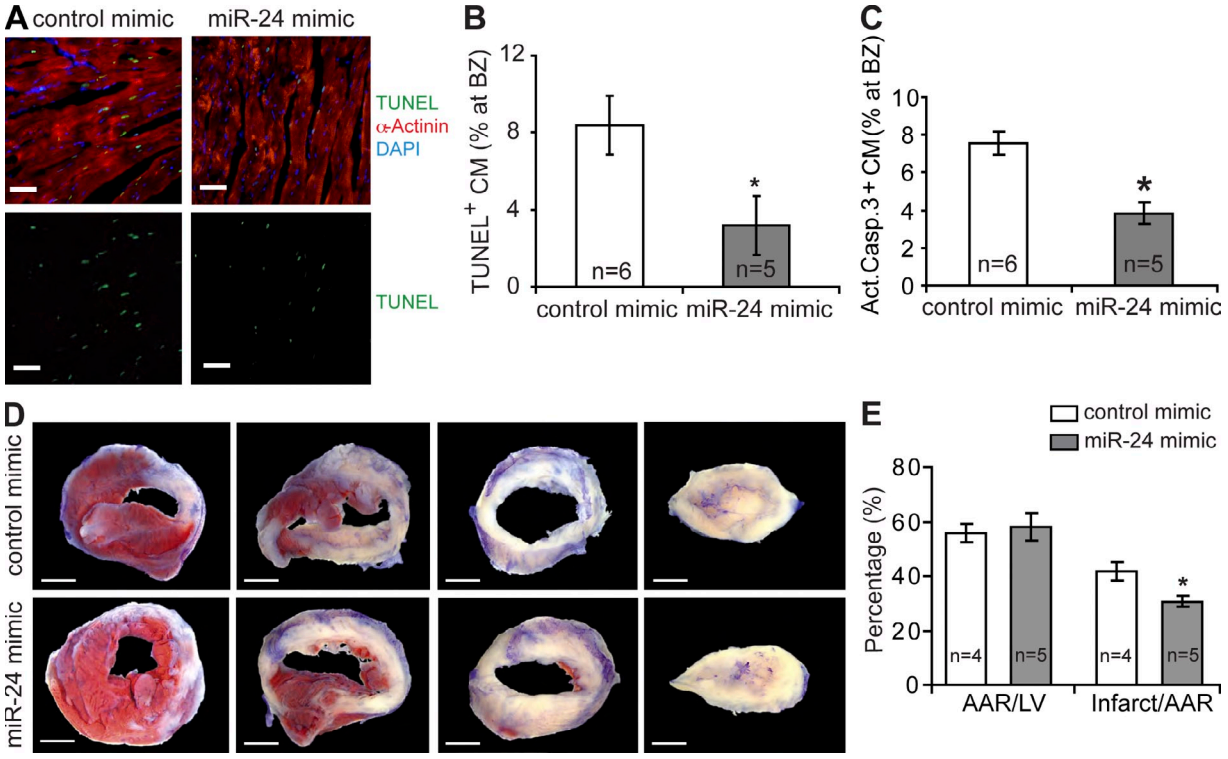

Figure 3. In vivo delivery of miR-24 inhibits apoptosis. (A and B) Immunohistochemistry of control mimic– or miR-24 mimic–treated heart sections marking TUNEL-positive cardiomyocytes costained with α-Actinin antibody within the BZ of infarcted hearts. Quantification is shown in B. (C) Quantification for activated Caspase 3^+ cardiomyocytes (CM) at BZ. (D) Representative pictures of Evans blue/TTC staining on four continuous slices of LV from representative hearts of control mimic– or miR-24 mimic–injected mouse. (E) Blinded quantification of size of the AAR and infarct size as described in Materials and methods. All staining in this figure was performed on hearts 24 h after MI. Measurements were repeated three times (technical triplicates), with biological sample size indicated in each panel. The mean number from technical triplicates was used for statistical calculation. Error bars indicate SEM (*, $P < 0.05$). Bars: (A) 50 µm; (D) 500 µm.

Published March 7, 2011

decrease in cardiac cell death by miR-24 would translate into improved heart function. Therefore, we assessed cardiac function 12 wk after MI by using magnetic resonance imaging (MRI). MRI revealed that the miR-24–treated mice had a higher ejection fraction (EF) and stroke volume (SV) than controls (Fig. 4 A). Moreover, cardiac output (the product of SV and heart rate) was increased in the miR-24 recipients (Fig. 4 A). This was attributable to better structure and contractility of the LV because heart rate was unaltered (Fig. S5 A). To monitor cardiac structure and function at several time

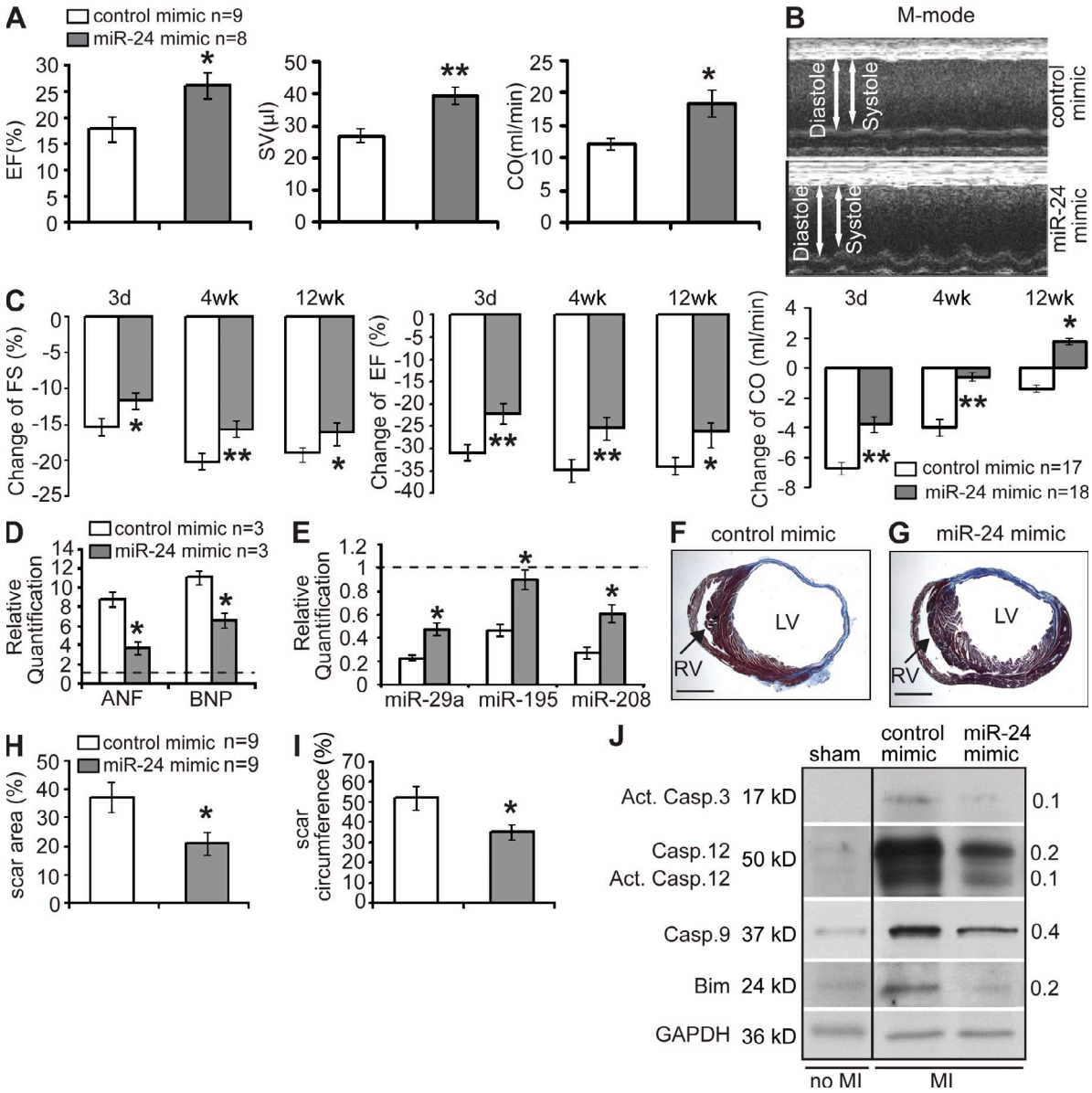

Figure 4. In vivo delivery of miR-24 blunts effects of MI. After MI, miR-24 or control mimic was injected along the BZ of infarct. (A) EF, SV, and cardiac output (CO) of the LV were measured by MRI 12 wk after MI. (B) M-mode echocardiography of representative hearts 3 d after MI. (C) Fractional shortening (FS), EF, and cardiac output at varying time points were measured using high-resolution echocardiography. Data were collected 1 d before and 3 d, 4 wk, and 12 wk after MI in a blinded fashion. (D) qPCR of ANF and BNP on RNA extracted from BZ of MI hearts 24 h after injection of control or miR-24 mimic. (E) Stress-responsive miRNAs were measured by qPCR 24 h after MI. Data in D and E are shown relative to control, indicated by dashed lines. (F and G) Azan staining was performed on heart sections 4 wk after MI with miR-24 or control mimic injected. RV, right ventricle. Bars, 500 μm. (H and I) Quantification of scar size was calculated by measurement of both scar area (H) and scar circumference (I). (J) Western blots for activated Caspase 3, Caspase 12, activated Caspase 12, Caspase 9, Bim, and GAPDH in protein extracts from control mimic– or miR-24 mimic–injected hearts 24 h after MI, as well as hearts without MI (sham). Relative quantification of Western blots is shown to the right of each panel; comparison was made between control mimic (set as 1) and miR-24 mimic after MI. The vertical black line indicates that intervening lanes have been spliced out. For all histograms, sample size (*n*) is indicated for each group. Each experiment was repeated three times (technical triplicates), and the mean number was used for statistical analyses. Error bars indicate SEM (*, $P < 0.05$; **, $P < 0.01$).

Published March 7, 2011

points after MI, we used high-resolution echocardiography (Fig. 4, B and C; and Fig. S5, B and C). miR-24– and control-treated mice underwent serial imaging 1 d before and 3 d, 4 wk, and 12 wk after MI. All mice showed a reduction in left ventricular function after coronary artery ligation, confirming successful induction of MI (Fig. 4, B and C; and Fig. S5 B). However, in mice treated with miR-24, the initial loss of contractility was significantly attenuated compared with controls (Fig. 4, B and C; and Fig. S5 B).

As a molecular readout of cardiac dysfunction, we performed qPCR to monitor the expression levels of atrial natriuretic factor (ANF) and brain natriuretic peptide (BNP) from miR-24–injected and control hearts. Both ANF and BNP were up-regulated 24 h after MI in controls as expected (Fig. 4 D). The up-regulation of ANF and BNP was attenuated by injection of miR-24 mimic in infarcted hearts (Fig. 4 D). We also assessed the expression level of a battery of stress-responsive miRNAs by qPCR. miR-29, miR-195, and miR-208 levels, which are dramatically reduced upon MI (van Rooij et al., 2006, 2007, 2008), were partially restored by overexpression of miR-24 (Fig. 4 E).

Consistent with the improvement of cardiac function, injection of miR-24 resulted in a smaller scar size 4 wk after MI (Fig. 4, F–I; and Fig. S5, D–F). Mice treated with miR-24 had a 33% reduction in scar circumference and a 46% reduction in scar area ($P < 0.05$; Fig. 4, F–I; and Fig. S5, D–F). Because stimulation of neovascularization could be another mechanism by which miR-24 decreased infarct size and improved cardiac function (van Laake et al., 2006), we quantified vascular density in the infarcted area, BZ, and distant myocardium. We found no difference in vessel formation between miR-24– and control-injected hearts (unpublished data).

miR-24 modulates apoptosis and suppresses Bim in vivo

Because our cell culture experiments (Figs. 1 and 2) demonstrated that miR-24 inhibited apoptosis and targeted the pro-apoptotic Bcl2 family protein Bim, we tested whether miR-24 regulated the same apoptosis pathway in vivo. Protein was extracted from the infarct zone (IZ) and BZ of mouse hearts 24 h after coronary ligation and injection with miR-24 mimic or control mimic. Consistent with its inhibitory role in apoptosis, miR-24 led to reduced protein levels of the final effector Caspase, activated Caspase 3, compared with controls after MI (Fig. 4 J). Caspase 8 was not significantly affected by miR-24 expression (not depicted); however, the increases in Caspase 12 and Caspase 9 were significantly attenuated in infarcted mouse hearts treated with miR-24 (Fig. 4 J). In addition, the increase in protein level of Bim after MI was dampened in these hearts compared with controls (Fig. 4 J).

Next we determined whether a decrease in Bim could mimic the in vivo effect of miR-24 expression on cardiomyocyte apoptosis. We delivered Bim small interfering RNA (siRNA) cocktails to the IZ and BZ of mouse hearts after coronary artery ligation. RNA and protein levels of Bim were measured to ensure efficient knockdown of *Bim* (Fig. S5, G and H). We found that inhibition of Bim expression resulted in less apoptosis at both the IZ and BZ of MI hearts 24 h after MI, as measured by TUNEL and activated Caspase 3 staining (Fig. 5, A and B; and not depicted).

To further investigate the relationship of miR-24 and *Bim*, we performed loss of function experiments of miR-24 by inhibiting endogenous miR-24 levels with Lipofectamine-mediated in vivo transfection of a miR-24 inhibitor, as described previously (Yang et al., 2007), with or without *Bim* knockdown. The miR-24 knockdown was confirmed by qPCR (Fig. S4 G). Inhibition of miR-24 resulted in increased apoptosis in BZ cardiomyocytes, increased expression of the downstream target *Bim*, and increased activity of Caspase 3, Caspase 12, and Caspase 9 (Fig. 5, C–E; and not depicted). Co-delivery of *Bim* siRNA and miR-24 inhibitor partially rescued the proapoptotic effects of miR-24 inhibition (Fig. 5, F and G; and not depicted).

DISCUSSION

In this study, we reveal a novel role for miR-24 in the regulation of mammalian cardiomyocyte apoptosis. We found that miR-24 inhibits apoptosis in cardiomyocytes in vitro and in vivo using a mouse MI model. In addition, we identified Bim as one of the direct targets of miR-24 and, through epistasis analyses, found that Bim mediates a part of miR-24's effect on apoptosis. Finally, introduction of miR-24 in vivo did not disturb the normal function of the heart but partially protected the heart from injury. The beneficial effects of miR-24 in MI hearts, while statistically significant by our measurement, are quite small and may be below the true sensitivity of the techniques being used. Future experimentation using more robust and accurate assays with a large sample number is needed for validation of applying this miRNA in treating ischemic cardiac disease. In addition, the improvement in heart function and reduction in scar size by overexpressing miR-24 might be caused by other functions of miR-24 independent of apoptosis or a combination of all. Further cardiac function analyses and scar size measurements when inhibiting the antiapoptotic function of miR-24 (i.e., knocking down the downstream components in miR-24–mediated apoptosis pathway) will hopefully provide some clues.

Like most miRNAs, miR-24 functions in many other biological processes and pathways. miR-24 was first reported to negatively regulate erythroid differentiation through inhibition of human activin type I receptor ALK4 (Wang et al., 2008). In addition, miR-24 appears to affect the tumor suppressor p16 (Lal et al., 2008), the DNA repair process, and cell cycle regulation (Lal et al., 2009a,b; Rogler et al., 2009). Particularly relevant to this study, miR-24 is required to prevent apoptosis during normal development of the retina in frogs (Walker and Harland, 2009), suggesting evolutionary conservation of miR-24 function, although the mechanisms may be divergent. These findings support the idea that a single miRNA, like miR-24, can regulate multiple independent pathways that may converge on a common biological outcome such as regulation of apoptosis. Other miRNAs, such as miR-21, may also play a role in regulating the cardiac

Published March 7, 2011

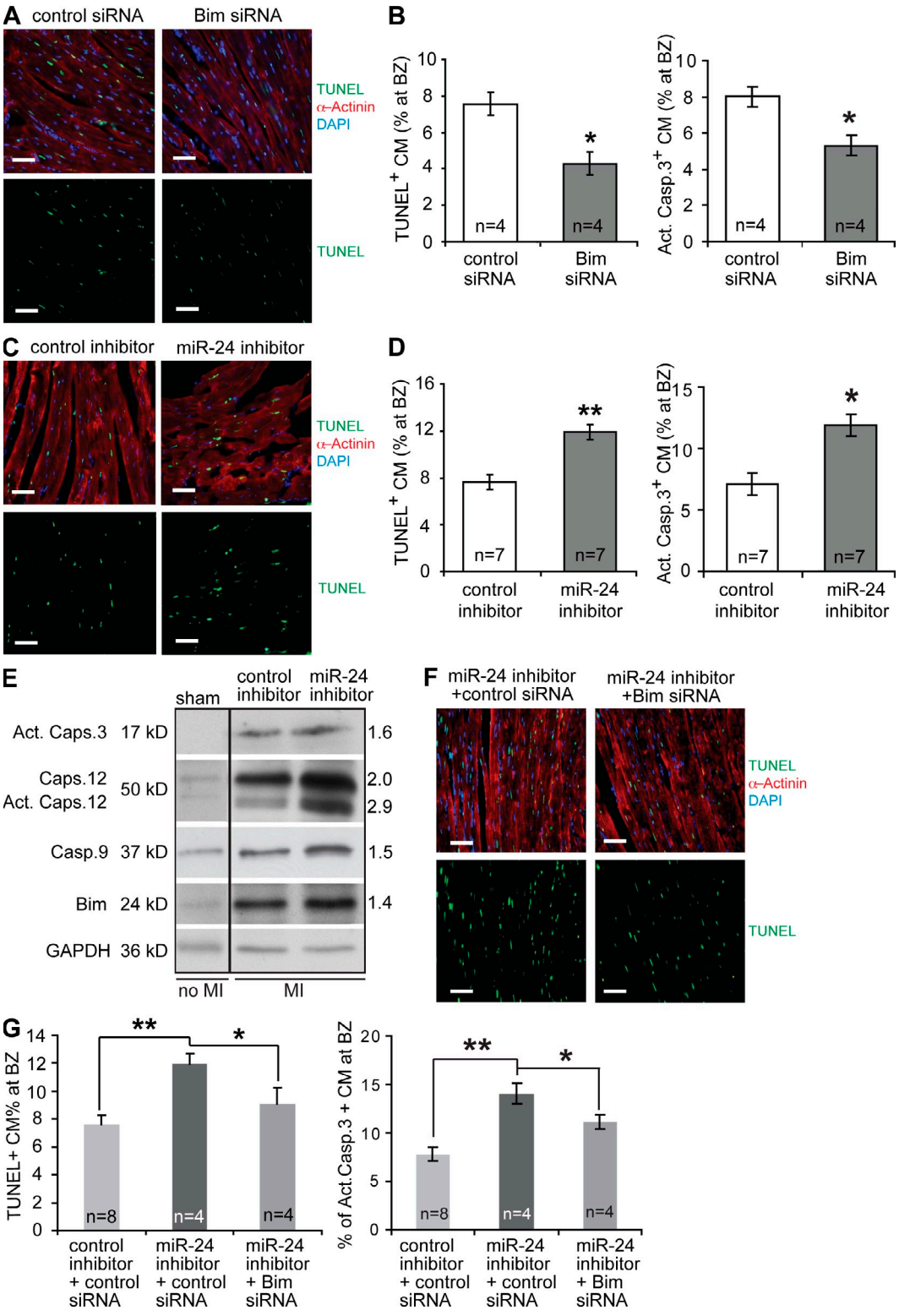

Figure 5. In vivo inhibition of *Bim* reduces miR-24 inhibitor–induced apoptosis. (A and B) After MI, control or *Bim* siRNA was injected along the BZ of infarct. Immunohistochemistry of heart sections labeling TUNEL-positive cardiomyocytes, marked by α-Actinin antibody within the BZ. DAPI indicates nuclei. Quantification of TUNEL+ or activated Caspase 3+ cells is shown in B. (C and D) Cardiomyocyte (CM) apoptosis was determined by TUNEL and activated Caspase 3 stainings on heart sections at the BZ of infarcted hearts with miR-24 or control inhibitor injected. (E) Western blots for activated Caspase 3, Caspase 12, activated Caspase 12, Caspase 9, Bim, and GAPDH in protein extracts from control inhibitor– or miR-24 inhibitor–injected hearts 24 h after MI, as well as hearts without MI (sham). Relative quantification of Western blots is shown to the right of each panel; comparison was made

Published March 7, 2011

response to ischemic injury (Thum et al., 2008; Dong et al., 2009).

miR-24 is expressed in both cardiomyocytes and fibroblasts. Our experiments demonstrate that miR-24 can exert antiapoptotic effects in cardiomyocytes in a cell-autonomous fashion. We and others have shown that cardiac fibroblasts can function as major signaling centers to affect the neighboring cardiomyocytes (Ieda et al., 2009; Takeda et al., 2010), and it is quite possible that miR-24 also functions in cardiac fibroblasts to promote cardiomyocyte survival. In this case, miR-24 would likely regulate pathways leading to paracrine secretion of survival factors that impinge on neighboring myocytes. Future studies of fibroblast-specific expression of miR-24 could help resolve this issue.

It is curious that an miRNA that represses an apoptotic factor such as Bim in the setting of ischemia would be down-regulated. One might expect that such an miRNA would be up-regulated to protect the cells from ischemic damage, particularly in the BZ which is attempting to survive in hypoxic conditions. However, the down-regulation may reflect the need to remove cells that are under ischemic stress. It will be interesting to determine whether the ischemia-induced miR-24 down-regulation has other more beneficial consequences through yet unknown targets.

The finding that miR-24 targets the Bcl2 family member Bim for repression highlights an important facet of miRNA-mediated regulation of critical cellular events. The dosage of Bim is apparently very important, as cells have engineered numerous mechanisms to quantitatively regulate its protein levels. Bim mediates both mitochondrial and ER stress–induced apoptosis and is regulated through multiple cellular modalities, including phosphorylation, ubiquitination, and proteosome-mediated degradation (Dijkers et al., 2000; Puthalakath and Strasser, 2002; Ley et al., 2005; Puthalakath et al., 2007). Our findings reveal yet another layer of posttranscriptional Bim regulation involving miR-24 and suggest that the cell uses numerous back-up mechanisms and regulatory pathways to carefully titrate the dose of this central regulator of apoptosis.

MATERIALS AND METHODS

Plasmid construction. Bim 3′ UTR was cloned from mouse genomic DNA and cardiomyocyte cDNA (Fig. S3 H) with the primers 5′-AGCGCTCTGCACTGTGTCGATGTGAACGG-3′ and 5′-ATGGCAGGGCTGTCAGGGATAGGGATGTC-3′. Amplified DNA was cloned into pCRII vector and subsequently cloned into pMIR-REPORT vector (Applied Biosystems). To express miR-24 in HeLa cells for luciferase assay, the genomic sequence containing premiR-24-2 plus flanking sequence (total ∼300 bp) were inserted into pEF-DEST51 (Invitrogen) with the primers 5′-CACCATCTCCTCAGGCCGCTGCTG-3′ and 5′-CTATCTGCTTTGGGGAACCACAG-3′. Site-directed PCR-mediated mutagenesis was performed using the QuikChange II XL Site-Directed Mutagenesis kit (Agilent Technologies). The following two pairs of primers were used to mutate both miR-24 binding sites in Bim 3′ UTR: 5′-CCCTGCAGTGGGAACGAAGACAGCTGATTTATAAGGC-3′ and 5′-GCCTTATAAATCAGCTGTCTTCGTTCCCACTGCAGGG-3′; and 5′-GTTTCACTCGTCAACGAAGACAAATGTCTCTGTGC-3′ and 5′-GCACAGAGACATTTGTCTTCGTTGACGAGTGAAAC-3′ (the underlined nucleotides are mutated ones).

Quantitative real-time PCR. RNA was extracted by the TRIZOL method (Invitrogen). RT-PCR was performed using the Superscript III first-strand synthesis system (Invitrogen). qPCR was performed using the ABI 7900HT (TaqMan; Applied Biosystems) per the manufacturer's protocols. Optimized primers from TaqMan Gene Expression Array were used. miRNA RT was conducted using the TaqMan MicroRNA Reverse Transcription kit (Applied Biosystems). miRNA real-time PCR (quantitative RT-PCR) was performed per the manufacturer's protocols by using primers from TaqMan MicroRNA assays (Applied Biosystems). Expression levels were normalized to Gapdh expression and RNU6 (miRNA qPCR).

Cell culture, transfection, and luciferase assay. Primary cardiomyocytes from mouse neonatal hearts were isolated and maintained as described previously (Ieda et al., 2009). Lipofectamine 2000 (Invitrogen)–mediated transfection was performed according to Invitrogen's protocol. miR-24 mimic (5′-UGGCUCAGUUCAGCAGGAACAG-3′), mimic control (5′-UUCUCCGAACGUGUCACGUTT-3′), miR24^{mut} mimic (5′-UGGCUCAGUUCAGUAAGAACCG-3′), miR-24 inhibitor (5′-ACCGAGUCAAGUCGUCCUUGUC-3′), inhibitor control (5′-UCUACUCUUUCUAGGAGGUUGUGA-3′), and miR24^{mut} inhibitor (5′-ACCGAGUCAAGUCAUUCUUGGC-3′; the underlined nucleotides are mutated ones) were purchased from Thermo Fisher Scientific and Shanghai GenePharma Co. For each transfection in 1 well of a 6-well plate, 40 pmol of mimic or inhibitor was used. For plasmid transfection, 100 ng of plasmid was transfected in 1 well of a 6-well plate. Luciferase assays were performed as described previously (Zhao et al., 2005) with the Dual-Luciferase reporter assay system (Promega).

Western blots and immunocytochemistry. Western blots were performed as described previously (Zhao et al., 2005). Mouse monoclonal anti–Caspase 8 (Sigma-Aldrich), mouse monoclonal anti–Caspase 9 (Sigma-Aldrich), rabbit anti–Caspase 3 (Sigma-Aldrich), rat monoclonal anti–Caspase 12 (Sigma-Aldrich), and rabbit polyclonal antibody against Bim (aa 4–195 of Bim$_{EL}$ form) were all used at a 1:1,000 dilution for Western blots. All Western blots were quantified using AlphaImager software (Alpha Innovations). Immunocytochemistry was performed according to a standard protocol. In brief, cells were fixed in 10% formalin (vol/vol) for 15 min on ice and washed with PBS twice. Cells were then incubated with primary antibody for 1 h at room temperature and washed with PBS three times and then incubated with secondary antibody for 0.5 h. After washing with PBS, cells were mounted in Vectashield with DAPI (Vector Laboratories). Mouse anti–α-Actinin was used at 1:400; guinea pig anti-Vimentin (Progen) was used at 1:200; rabbit anti–Caspase 3 (Sigma-Aldrich) was used at 1:200 for immunocytochemistry. Alexa Fluor 546 or Alexa Fluor 488 anti–mouse (Invitrogen) was used at 1:200 as secondary antibody. TUNEL staining was performed using the In Situ Cell Death Detection kit, Fluorescein (Roche) per the manufacturer's protocol.

Flow cytometry. For FACS analysis to detect early apoptotic cells (AnnexinV$^+$PI$^-$), 5×10^5 dissociated cells were washed twice in PBS and resuspended in 1× binding buffer (BD). Then the cells were stained with 1 µl AnnexinV-FITC and 0.5 µl PI (BD) for 30 min in the dark and followed by FACS analysis with FACSCalibur (BD). For FACS analysis of cell cycle, dissociated cells were fixed and permeabilized by cold 70% ethanol (overnight

between control inhibitor (set as 1) and miR-24 inhibitor after MI. The vertical black line indicates that intervening lanes have been spliced out. (F) TUNEL stainings on MI heart sections coinjected with *Bim* siRNA or control siRNA and miR-24 inhibitor. (G) Quantification of TUNEL$^+$ or activated Caspase 3$^+$ cardiomyocytes. All experiments were repeated three times (technical triplicates), with biological duplicates indicated in each panel. Error bars indicate SEM (*, $P < 0.05$; **, $P < 0.01$). All data in this figure were collected 24 h after MI. Bars, 50 µm.

Published March 7, 2011

at 4°C). Subsequently, 10 µl of 500 µg/ml RNase and 10 µl of 1 mg/ml PI were added to resuspended cells and incubated at 37°C for 30 min in the dark. After washing with PBS twice, stained cells were analyzed by FACS-Calibur. For FACS sorting of endothelial cells, dissociated cells from mouse hearts were stained with FITC rat anti–mouse CD31 (BD) for 30 min at room temperature. After washing with PBS twice, stained cells were sorted by Aria (BD).

Mouse MI model. The protocol was approved by institutional guidelines (University of California, San Francisco Institutional Animal Care and Use Committee). All surgeries and subsequent analyses were performed in a blinded fashion for genotype and intervention. Mice were anesthetized with 2.4% isoflurane/97.6% oxygen and placed in a supine position on a heating pad (37°C). Animals were intubated with a 19-gauge stump needle and ventilated with room air with a MiniVent Type 845 mouse ventilator (Hugo Sachs Elektronik-Harvard Apparatus; SV, 250 µl; respiratory rate, 120 breaths/min). MI was induced by permanent ligation of the left anterior descending artery with a 7-0 Prolene suture as described previously (Bock-Marquette et al., 2004). Sham-operated animals served as surgical controls and were subjected to the same procedures as the experimental animals with the exception that the left anterior descending artery was not ligated. All surgical procedures were performed under aseptic conditions. 4 wk or 24 h after occlusion, the heart was removed for perfusion fix (4% paraformaldehyde [PFA]; paraffin sections for structural analysis and immunohistochemistry) or immersion fix (0.5% PFA in 5% sucrose; cryo sections for immunofluorescent staining), or the tissues within the IZ, BZ, and nonischemic zone distal to the IZ (DZ) were dissected for RNA or protein isolation.

Determination of the AAR and myocardial infarct size. 24 h after coronary ligation, the mice were anesthetized and cannulated with tubing. 2% Evans blue (Sigma-Aldrich) was perfused into the aorta; thus, all myocardial tissue was stained blue except the AAR. The LV was isolated and cut into four ∼1-mm pieces with the first cut at the ligation level. LV slices were stained in 1.5% TTC for 30 min at 37°C and then fixed in 4% PFA overnight at 4°C. The area of infarction was demarcated as a white area, whereas viable myocardium was stained red. Photographs were taken for both sides of each section. The AAR and the infarct area were determined via planimetry by using the computer software ImagePro (Bio-Rad Laboratories). Infarct size was calculated as the percentage of MI compared with the AAR using a previously described methodology (Kurrelmeyer et al., 2000).

In vivo delivery of miR-24 mimic, inhibitor, and Bim siRNA. With the chest open, oligonucleotides stabilized with 2′-O-methyl modification pretreated with 20 µl Lipofectamine 2000 were injected into the myocardium through an insulin syringe with incorporated 29-gauge needle (BD) into the myocardium. The dosages used per mouse were 40 ng miR-24 mimic, 40 ng control mimic, 80 ng miR-24 inhibitor, 80 ng inhibitor control (Shanghai GenePharma Co.), 3 nmol Bim siRNAs (a pool of three target-specific 20–25 nt siRNAs; Santa Cruz Biotechnology, Inc.), or 3 nmol negative control siRNAs (Santa Cruz Biotechnology, Inc.). For each type of oligonucleotide, one injection with a full dosage was used along the boundary between the IZ and BZ (based on the blanched infarct area) after coronary artery occlusion. After injection, the chest was closed with sutures, and the mouse was allowed to recover with mouse ventilator and heating pad.

Echocardiography. Echocardiography was performed by the Vevo 770 High-Resolution Micro-Imaging System (VisualSonics) with a 15-MHz linear array ultrasound transducer. The LV was assessed in both parasternal long- and short-axis views at a frame rate of 120 Hz. End systole or end diastole was defined as the phase in which the smallest or largest area of LV, respectively, was obtained. Left ventricular end systolic diameter and left ventricular end diastolic diameter were measured from the LV M-mode tracing with a sweep speed of 50 mm/s at the papillary muscle level.

MRI. MRI was performed on a small animal scanner (DirectDrive 7T; Varian). Each mouse was anesthetized by inhalation of 2% isoflurane/98% oxygen administered via an MRI-compatible mobile inhalation anesthesia system (VetEquip) and maintained at 37°C. Two electrocardiography (ECG) leads were inserted into the right front and left rear leg. ECG waveforms were monitored with a small animal monitoring and gating system (SA Instruments). The mouse was then placed into a homemade 1H birdcage coil with an inner diameter of 32 mm. A group of ECG (R-wave rising edge)-triggered spin echo scout images were acquired first to define the oblique plane of the short axis. Then an ECG-triggered two-dimensional gradient echo sequence with an echo time of 2.75 ms, repetition time of 200 ms, and a flip angle of 45° was used to obtain cine short-axis images at 12 or 13 phases per cardiac cycle. Each scan consisted of eight to nine contiguous slices spanning LV from apex to base with 1-mm thickness, a matrix size of 128 × 128, a field of view of 25.6 × 25.6 mm, and four means.

Immunohistochemistry on mouse hearts. After perfusion fix, the heart was removed and fixed by immersion in 4% PFA in PBS (diluted from 20% PFA stock; Electron Microscopy Sciences) and routinely processed and paraffin embedded. 5-µm sections were stained with hematoxylin and eosin and analyzed for regular morphology. To measure the infarct size at 4 wk after MI, LVs were cut from apex to base; sections from four equally distributed levels were Azan or Masson's trichrome stained. Scar size was calculated as the percentage of the LV circumference, or total scar area divided by total LV area, and was summed from four transverse sections per heart. Adjacent sections were used to quantify vascular density after staining with PECAM-1 antibody (rat; 1:20; BD) as described previously (van Laake et al., 2006). To quantify apoptotic cardiomyocytes, mouse hearts were removed 24 h after coronary artery ligation, fixed with 0.5% PFA in 5% sucrose, and routinely frozen embedded in OCT and processed for sectioning and staining with Caspase 3 (1:200) or TUNEL and α-Actinin (mouse; 1:800; Sigma-Aldrich) as described previously (van Laake et al., 2008). TUNEL was performed using an In Situ Cell Death Detection kit, Fluorescein (Roche) per the manufacturer's protocol. DAPI was used for nuclear counterstaining. Frozen heart sections were also stained with pH3 (rabbit; 1:100; Millipore), α-Actinin, and DAPI to quantify proliferating cardiomyocytes.

Statistics. For echocardiography, MRI, TUNEL, Azan, Masson's trichrome, Evans blue/TTC, and PECAM-1 staining quantification, statistical analysis was performed using SPSS version 15. Comparisons between groups were made by one-way analysis of variance or Mann–Whitney U test, as applicable. Sample numbers were indicated in corresponding figures. For quantitative RT-PCR, FACS, and luciferase assay, we used biological triplicates and technical triplicates; data were analyzed by unpaired Student's *t* test. Error bars indicate SEM. *, $P < 0.05$; **, $P < 0.01$.

Online supplemental material. Fig. S1 shows qPCR for miR-23 and miR-27 in MI heart and the expression pattern of miR-24. Fig. S2 shows validation for miR-24 mimic and inhibitor transfection in primary cardiomyocytes. Fig. S3 shows that miR-24 regulates apoptosis but not cell cycle and miR-24 regulates Bim in cardiomyocytes. Fig. S4 shows validation for miR-24 mimic and inhibitor in vivo transfection. Fig. S5 shows additional MRI and echo data, Masson's trichrome staining on hearts 4 wk after MI, and validation for Bim siRNA knockdown. Online supplemental material is available at http://www.jem.org/cgi/content/full/jem.20101547/DC1.

We are grateful for expert technical assistance from the Gladstone Stem Cell Core (J. Arnold and K.N. Ivey), Flow Cytometry Core (S. Elmes), and Genomics Core (L. Ta, Y. Hao, and C.S. Barker). We thank all of the members of the Srivastava laboratory for helpful discussion.

L. Qian is a postdoctoral scholar of the California Institute for Regenerative Medicine. D. Srivastava was supported by grants from the National Heart, Lung and Blood Institute/National Institutes of Health, the California Institute for Regenerative Medicine, and the Younger Family Foundation. L.W. van Laake was supported by an Interuniversity Cardiology Institute of the Netherlands fellowship grant. This work was supported by National Institutes of Health/National Center for Research Resources grant C06 RR018928 to the Gladstone Institute of Cardiovascular Diseases.

The authors have no conflicting financial interests.

Submitted: 30 July 2010
Accepted: 2 February 2011

REFERENCES

Ambros, V. 2003. MicroRNA pathways in flies and worms: growth, death, fat, stress, and timing. *Cell*. 113:673–676. doi:10.1016/S0092-8674(03)00428-8

Bartel, D.P. 2009. MicroRNAs: target recognition and regulatory functions. *Cell*. 136:215–233. doi:10.1016/j.cell.2009.01.002

Bock-Marquette, I., A. Saxena, M.D. White, J.M. Dimaio, and D. Srivastava. 2004. Thymosin beta4 activates integrin-linked kinase and promotes cardiac cell migration, survival and cardiac repair. *Nature*. 432:466–472. doi:10.1038/nature03000

Carè, A., D. Catalucci, F. Felicetti, D. Bonci, A. Addario, P. Gallo, M.L. Bang, P. Segnalini, Y. Gu, N.D. Dalton, et al. 2007. MicroRNA-133 controls cardiac hypertrophy. *Nat. Med.* 13:613–618. doi:10.1038/nm1582

Chen, J.F., E.M. Mandel, J.M. Thomson, Q. Wu, T.E. Callis, S.M. Hammond, F.L. Conlon, and D.Z. Wang. 2006. The role of microRNA-1 and microRNA-133 in skeletal muscle proliferation and differentiation. *Nat. Genet.* 38:228–233. doi:10.1038/ng1725

Dijkers, P.F., R.H. Medema, J.W. Lammers, L. Koenderman, and P.J. Coffer. 2000. Expression of the pro-apoptotic Bcl-2 family member Bim is regulated by the forkhead transcription factor FKHR-L1. *Curr. Biol.* 10:1201–1204. doi:10.1016/S0960-9822(00)00728-4

Dong, S., Y. Cheng, J. Yang, J. Li, X. Liu, X. Wang, D. Wang, T.J. Krall, E.S. Delphin, and C. Zhang. 2009. MicroRNA expression signature and the role of microRNA-21 in the early phase of acute myocardial infarction. *J. Biol. Chem.* 284:29514–29525. doi:10.1074/jbc.M109.027896

Hengartner, M.O. 2000. The biochemistry of apoptosis. *Nature*. 407:770–776. doi:10.1038/35037710

Ieda, M., T. Tsuchihashi, K.N. Ivey, R.S. Ross, T.T. Hong, R.M. Shaw, and D. Srivastava. 2009. Cardiac fibroblasts regulate myocardial proliferation through beta1 integrin signaling. *Dev. Cell.* 16:233–244. doi:10.1016/j.devcel.2008.12.007

Ivey, K.N., A. Muth, J. Arnold, F.W. King, R.F. Yeh, J.E. Fish, E.C. Hsiao, R.J. Schwartz, B.R. Conklin, H.S. Bernstein, and D. Srivastava. 2008. MicroRNA regulation of cell lineages in mouse and human embryonic stem cells. *Cell Stem Cell*. 2:219–229. doi:10.1016/j.stem.2008.01.016

Kang, P.M., A. Haunstetter, H. Aoki, A. Usheva, and S. Izumo. 2000. Morphological and molecular characterization of adult cardiomyocyte apoptosis during hypoxia and reoxygenation. *Circ. Res.* 87:118–125.

Kitsis, R.N., C.F. Peng, and A.M. Cuervo. 2007. Eat your heart out. *Nat. Med.* 13:539–541. doi:10.1038/nm0507-539

Krek, A., D. Grün, M.N. Poy, R. Wolf, L. Rosenberg, E.J. Epstein, P. MacMenamin, I. da Piedade, K.C. Gunsalus, M. Stoffel, and N. Rajewsky. 2005. Combinatorial microRNA target predictions. *Nat. Genet.* 37:495–500. doi:10.1038/ng1536

Kurrelmeyer, K.M., L.H. Michael, G. Baumgarten, G.E. Taffet, J.J. Peschon, N. Sivasubramanian, M.L. Entman, and D.L. Mann. 2000. Endogenous tumor necrosis factor protects the adult cardiac myocyte against ischemic-induced apoptosis in a murine model of acute myocardial infarction. *Proc. Natl. Acad. Sci. USA*. 97:5456–5461. doi:10.1073/pnas.070036297

Kwon, C., Z. Han, E.N. Olson, and D. Srivastava. 2005. MicroRNA1 influences cardiac differentiation in *Drosophila* and regulates Notch signaling. *Proc. Natl. Acad. Sci. USA*. 102:18986–18991. doi:10.1073/pnas.0509535102

Lal, A., H.H. Kim, K. Abdelmohsen, Y. Kuwano, R. Pullmann Jr., S. Srikantan, R. Subrahmanyam, J.L. Martindale, X. Yang, F. Ahmed, et al. 2008. p16(INK4a) translation suppressed by miR-24. *PLoS ONE*. 3:e1864. doi:10.1371/journal.pone.0001864

Lal, A., F. Navarro, C.A. Maher, L.E. Maliszewski, N. Yan, E. O'Day, D. Chowdhury, D.M. Dykxhoorn, P. Tsai, O. Hofmann, et al. 2009a. miR-24 Inhibits cell proliferation by targeting E2F2, MYC, and other cell-cycle genes via binding to "seedless" 3'UTR microRNA recognition elements. *Mol. Cell*. 35:610–625. doi:10.1016/j.molcel.2009.08.020

Lal, A., Y. Pan, F. Navarro, D.M. Dykxhoorn, L. Moreau, E. Meire, Z. Bentwich, J. Lieberman, and D. Chowdhury. 2009b. miR-24-mediated downregulation of H2AX suppresses DNA repair in terminally differentiated blood cells. *Nat. Struct. Mol. Biol.* 16:492–498. doi:10.1038/nsmb.1589

Ley, R., K.E. Ewings, K. Hadfield, and S.J. Cook. 2005. Regulatory phosphorylation of Bim: sorting out the ERK from the JNK. *Cell Death Differ.* 12:1008–1014. doi:10.1038/sj.cdd.4401688

Lutgens, E., M.J. Daemen, E.D. de Muinck, J. Debets, P. Leenders, and J.F. Smits. 1999. Chronic myocardial infarction in the mouse: cardiac structural and functional changes. *Cardiovasc. Res.* 41:586–593. doi:10.1016/S0008-6363(98)00216-8

Mackman, N. 2008. Triggers, targets and treatments for thrombosis. *Nature*. 451:914–918. doi:10.1038/nature06797

Puthalakath, H., and A. Strasser. 2002. Keeping killers on a tight leash: transcriptional and post-translational control of the pro-apoptotic activity of BH3-only proteins. *Cell Death Differ.* 9:505–512. doi:10.1038/sj.cdd.4400998

Puthalakath, H., L.A. O'Reilly, P. Gunn, L. Lee, P.N. Kelly, N.D. Huntington, P.D. Hughes, E.M. Michalak, J. McKimm-Breschkin, N. Motoyama, et al. 2007. ER stress triggers apoptosis by activating BH3-only protein Bim. *Cell*. 129:1337–1349. doi:10.1016/j.cell.2007.04.027

Rajewsky, N. 2006. microRNA target predictions in animals. *Nat. Genet.* 38:S8–S13. doi:10.1038/ng1798

Rogler, C.E., L. Levoci, T. Ader, A. Massimi, T. Tchaikovskaya, R. Norel, and L.E. Rogler. 2009. MicroRNA-23b cluster microRNAs regulate transforming growth factor-beta/bone morphogenetic protein signaling and liver stem cell differentiation by targeting Smads. *Hepatology*. 50:575–584. doi:10.1002/hep.22982

Ruvkun, G. 2008. The perfect storm of tiny RNAs. *Nat. Med.* 14:1041–1045. doi:10.1038/nm1008-1041

Sokol, N.S., and V. Ambros. 2005. Mesodermally expressed *Drosophila* microRNA-1 is regulated by Twist and is required in muscles during larval growth. *Genes Dev.* 19:2343–2354. doi:10.1101/gad.1356105

Swynghedauw, B. 1999. Molecular mechanisms of myocardial remodeling. *Physiol. Rev.* 79:215–262.

Takeda, N., I. Manabe, Y. Uchino, K. Eguchi, S. Matsumoto, S. Nishimura, T. Shindo, M. Sano, K. Otsu, P. Snider, et al. 2010. Cardiac fibroblasts are essential for the adaptive response of the murine heart to pressure overload. *J. Clin. Invest.* 120:254–265. doi:10.1172/JCI40295

Thum, T., C. Gross, J. Fiedler, T. Fischer, S. Kissler, M. Bussen, P. Galuppo, S. Just, W. Rottbauer, S. Frantz, et al. 2008. MicroRNA-21 contributes to myocardial disease by stimulating MAP kinase signalling in fibroblasts. *Nature*. 456:980–984. doi:10.1038/nature07511

van Laake, L.W., S. van den Driesche, S. Post, A. Feijen, M.A. Jansen, M.H. Driessens, J.J. Mager, R.J. Snijder, C.J. Westermann, P.A. Doevendans, et al. 2006. Endoglin has a crucial role in blood cell-mediated vascular repair. *Circulation*. 114:2288–2297. doi:10.1161/CIRCULATIONAHA.106.639161

van Laake, L.W., R. Passier, P.A. Doevendans, and C.L. Mummery. 2008. Human embryonic stem cell-derived cardiomyocytes and cardiac repair in rodents. *Circ. Res.* 102:1008–1010. doi:10.1161/CIRCRESAHA.108.175505

van Rooij, E., L.B. Sutherland, N. Liu, A.H. Williams, J. McAnally, R.D. Gerard, J.A. Richardson, and E.N. Olson. 2006. A signature pattern of stress-responsive microRNAs that can evoke cardiac hypertrophy and heart failure. *Proc. Natl. Acad. Sci. USA*. 103:18255–18260. doi:10.1073/pnas.0608791103

van Rooij, E., L.B. Sutherland, X. Qi, J.A. Richardson, J. Hill, and E.N. Olson. 2007. Control of stress-dependent cardiac growth and gene expression by a microRNA. *Science*. 316:575–579. doi:10.1126/science.1139089

van Rooij, E., L.B. Sutherland, J.E. Thatcher, J.M. DiMaio, R.H. Naseem, W.S. Marshall, J.A. Hill, and E.N. Olson. 2008. Dysregulation of microRNAs after myocardial infarction reveals a role of miR-29 in cardiac fibrosis. *Proc. Natl. Acad. Sci. USA*. 105:13027–13032. doi:10.1073/pnas.0805038105

Ventura, A., A.G. Young, M.M. Winslow, L. Lintault, A. Meissner, S.J. Erkeland, J. Newman, R.T. Bronson, D. Crowley, J.R. Stone, et al. 2008. Targeted deletion reveals essential and overlapping functions of the miR-17 through 92 family of miRNA clusters. *Cell*. 132:875–886. doi:10.1016/j.cell.2008.02.019

Walker, J.C., and R.M. Harland. 2009. microRNA-24a is required to repress apoptosis in the developing neural retina. *Genes Dev.* 23:1046–1051. doi:10.1101/gad.1777709

Published March 7, 2011

Wang, Q., Z. Huang, H. Xue, C. Jin, X.L. Ju, J.D. Han, and Y.G. Chen. 2008. MicroRNA miR-24 inhibits erythropoiesis by targeting activin type I receptor ALK4. *Blood*. 111:588–595. doi:10.1182/blood-2007-05-092718

Xiao, C., L. Srinivasan, D.P. Calado, H.C. Patterson, B. Zhang, J. Wang, J.M. Henderson, J.L. Kutok, and K. Rajewsky. 2008. Lymphoproliferative disease and autoimmunity in mice with increased miR-17-92 expression in lymphocytes. *Nat. Immunol.* 9:405–414. doi:10.1038/ni1575

Yang, B., H. Lin, J. Xiao, Y. Lu, X. Luo, B. Li, Y. Zhang, C. Xu, Y. Bai, H. Wang, et al. 2007. The muscle-specific microRNA miR-1 regulates cardiac arrhythmogenic potential by targeting GJA1 and KCNJ2. *Nat. Med.* 13:486–491. doi:10.1038/nm1569

Zhao, Y., and D. Srivastava. 2007. A developmental view of microRNA function. *Trends Biochem. Sci.* 32:189–197. doi:10.1016/j.tibs.2007.02.006

Zhao, Y., E. Samal, and D. Srivastava. 2005. Serum response factor regulates a muscle-specific microRNA that targets Hand2 during cardiogenesis. *Nature*. 436:214–220. doi:10.1038/nature03817

Zhao, Y., J.F. Ransom, A. Li, V. Vedantham, M. von Drehle, A.N. Muth, T. Tsuchihashi, M.T. McManus, R.J. Schwartz, and D. Srivastava. 2007. Dysregulation of cardiogenesis, cardiac conduction, and cell cycle in mice lacking miRNA-1-2. *Cell*. 129:303–317. doi:10.1016/j.cell.2007.03.030